ACUSTICA · acta acustica
Vol. 83 (1997) 59 – 66

The Subharmonic Oscillations And Combination-Frequency Subharmonic Emissions From A Resonant Bubble: Their Properties and Generation Mechanisms

A. D. Phelps, T. G. Leighton
The Institute of Sound and Vibration Research, The University of Southampton, Southampton SO17 1BJ, UK

Summary
Sizing bubbles using a two frequency technique which examines the coupling of a resonant subharmonic oscillation to an imaging beam is not prone to some of the inaccuracies and ambiguities of other methods. This combination frequency subharmonic signal is parametric in nature, and the amplitude onset threshold has been quantified for thirty tethered air bubbles in water. This paper details work which aims to investigate the generation mechanism of a bubble's subharmonic oscillations, and presents results from theoretical consideration of three potential mechanisms: (i) The possibility that at high amplitudes a bifurcation appears in a bubble's volumetric pulsations; (ii) the potential for bubbles driven at twice their resonant frequency to pulsate with a component at their resonant frequency (which is a subharmonic of the driving field); (iii) that surface waves are responsible. The first two mechanisms are examined using a numerical solution to the Gilmore-Akulichev model, and the third us ing plane surface theory. Whilst all three mechanisms show the potential for generating subharmonic oscillations, the first two demonstrate onset thresholds four and three orders of magnitude higher than the experimental threshold respectively. However, the threshold predicted using surface wave theory shows very good agreement with the experimental results.

PACS no. 43.30.Lz, 43.25.Yw

1. Introduction

The applications of bubble detection and sizing are required in many seemingly diverse fields of study, including industrial processes, medical science and investigations into the oceanic environment [1, 2, 3]. Often the most appropriate way of measuring bubbles utilises their strong acoustic scattering properties caused by the large impedance mismatch at their surface, and the fact that bubbles pulsate when driven by a sound field with a resonance frequency ν_0 given by:

$$\nu_0 = \frac{1}{2\pi R_0\sqrt{\rho}}\sqrt{3\kappa\left(p_0 + \frac{2\sigma}{R_0}\right) - \frac{2\sigma}{R_0} - \frac{4\mu^2}{\rho R_o^2}}, \qquad (1)$$

where R_0 is the bubble's equilibrium radius, ρ is the density of the surrounding fluid, p_0 is the hydrostatic pressure around the bubble, σ is the surface tension, μ is the shear viscosity coefficient and κ is the polytropic index of the pulsations of the gas inside the bubble [4, 5]. Thus a knowledge of the resonance frequency of the bubble can be used to infer its size.

The acoustically driven pulsations of a bubble are inherently nonlinear at high amplitude, a state which is typically taken to indicate resonant activity. Thus the appearance of nonlinear behaviour has been used as a more accurate measure of the bubble resonance frequency than by just examining the strength of the linear backscatter, which may not be a maximum at resonance [6]. The most basic form of these nonlinearities is the presence of harmonics of a tonal driving frequency ω_p, with signals at $2\omega_p$, $3\omega_p$, etc. However, in addition to these harmonic frequencies, ultraharmonic signals at $3\omega_p/2, 5\omega_p/2$ etc. and subharmonic signals at $\omega_p/2, \omega_p/3$ etc. have also been observed [7, 8]. The most prominent of these non-integer harmonic signals is the order 1/2 subharmonic, which differs from the basic harmonic behaviour in that it is parametric in nature, i.e. it is a threshold phenomenon as the signal only appears above a particular driving amplitude. The oscillation at $\omega_p/2$ has been the subject of recent research, as it has been observed to couple effectively with an imaging beam giving rise to combination frequency components: as the subharmonic oscillation arises through higher order nonlinear behaviour, the combination frequency subharmonic emission has been shown to be a much more accurate indicator of a bubble resonance, and not to be prone to the ambiguities of other methods [9, 10].

Clearly the combination frequency subharmonic emission used in bubble measurement procedures must result from some subharmonic component in the bubble oscillation. To date, however, proof of the actual mechanism by which the uncombined subharmonic emission arises from stable cavitation is unavailable. Previously, however, it had been theorised that the emission arises from bubbles which are driven at twice their resonance frequency [11, 12], as small perturbation analysis demonstrates that a bubble will pulsate slightly at its resonance frequency under these conditions: this emission occurs at a subharmonic of the driving frequency. Additionally it has been postulated that the emission may be brought about by surface waves set up around the bubble wall [13], although he noted that it is unlikely that these signals would carry to distance in the fluid as the volume of the bubble does not change.

This paper describes the results from work undertaken to investigate the source of the subharmonic bubble signals. Using experimental techniques, which are described elsewhere [10, 14], the amplitude threshold for the combination frequency subharmonic signals has been accurately quantified for thirty air bubbles in water resonant in the range 2000 Hz to 3200 Hz. This must be the same onset threshold for the

Received 25 October 1995,
accepted 27 March 1996.

ACUSTICA · acta acustica
Vol. 83 (1997)

pertinent bubble oscillations at the subharmonic frequency, which are the mechanism for the generation of the combination frequency subharmonic acoustic emissions. Using this onset threshold value, three potential sources for the subharmonic bubble oscillation are investigated. The first is the possibility that a bifurcation occurs in the resonant volumetric pulsations of the bubble giving alternate maxima in the radius-time curves. The second possible mechanism looks at the large bubble theory mentioned above, where bubbles driven at twice their resonance frequency pulsate slightly at their resonance, which shows as a subharmonic of the driving sound field. The third mechanism involves the onset of surface waves around the bubble wall. The first two mechanisms were investigated using a bubble dynamics model based on the Gilmore equation of motion, and the third applies theory derived for flat surfaces to the problem, which is approximately valid for the small wavelength surface oscillations when compared with the circumference of the bubble.

2. Brief Summary Of The Experimental Results

The experimental work is extensively described elsewhere [10, 14], and so only a brief outline of the methodology and results will be presented here. For all the results discussed in the text, the sinusoidal pressure levels of the driving sound fields are given in Pa (0-pk), i.e. the amplitude of the sine wave. The bubble measurement procedure used a two frequency technique to investigate the response of air bubbles in water, where the bubble is simultaneously excited with a *pump* beam and an *imaging* beam. The pump signal, at ω_p, is variable in frequency and is incremented through the speculative location of the bubble's resonant frequency in discrete frequency steps. The imaging beam has a fixed frequency (ω_i) which is considerably higher than the bubble resonance frequency, being of the MHz order, and is used to continuously insonify the bubble. When the bubble undergoes the high amplitude nonlinear pulsations at resonance, the two signals are coupled together. This is demonstrated in Figure 1(a) with data taken from a tethered bubble insonified at resonance at a pump signal amplitude of 25 Pa. It can be seen that the signal returned from the bubble consists of the imaging frequency (which, as it is considerably higher in frequency, plots so densely as to appear continuously black), amplitude modulated by the pump/resonance frequency. This gives rise to signals at frequencies of $\omega_i + \omega_p$ and $\omega_i - \omega_p$. Thus by investigating the returned signal content around the imaging frequency for these sum-and-difference frequency components the bubble resonance can be determined [15]. Ideally, the returned signal would contain only bubble mediated information, and thus would be able to distinguish between direct sound transfer from the projector to the receiver, nonlinearities in the generation/measuring equipment etc. It would also enable the bubble information to be investigated in a 'quieter' frequency window rather than in the high ambient noise window around the bubble's resonance.

It was discovered, however, that the appearance of these direct coupled sum-and-difference signals was not an unambiguous indicator of high amplitude bubble activity, as the nonlinear mixing could be brought on through non-bubble effects such as turbulence and the modulation of the high frequency receiver source by the projector sound field [16]. Additionally, it was limited in its accuracy as bubbles insonified far off resonance could still contribute a direct coupled signal. This is because the returned signal can be considered as the output from a cyclo-stationary process, where it is a measure of the acoustic cross section of a pulsating target. Therefore if the bubble volume changes at all as a result of the application of the pump sound field, which it will do off-resonance, the returned signal will then comprise the imaging signal amplitude modulated by the pumping frequency; this will give $\omega_i \pm \omega_p$ signal components. However, it was also discovered that the bubble's subharmonic oscillation also underwent sum-and-difference coupling to give a much more accurate and unambiguous indicator of the resonance of a given bubble. This is demonstrated in Figure 1(b), which is taken from the same bubble as shown in Figure 1(a), but

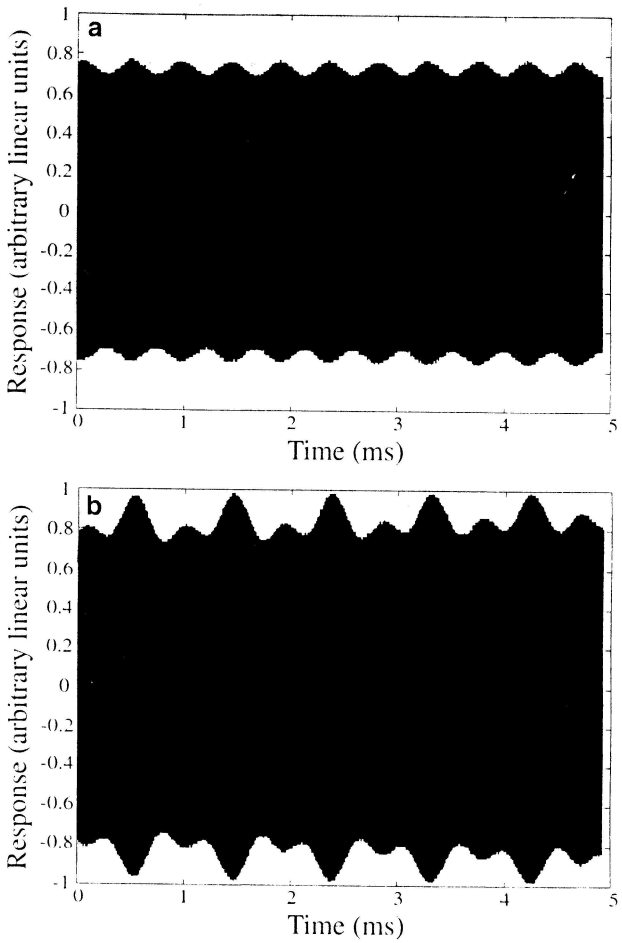

Figure 1. Returned signals from a bubble insonified at two frequencies measured with a high frequency probe – the high frequency imaging signal was set at 1.1 MHz, and the bubble resonance/pump frequency at 2160 Hz. The data was sampled at 10 MHz on a LeCroy 9314L digital oscilloscope. Plot (a) shows the sum-and-difference direct coupling by a bubble excited at 25 Pa (0-pk), whereas plot (b) shows the emergence of the subharmonic sum-and-difference signal from the same bubble driven at 40 Pa (0-pk). The high imaging frequency plots so densely as to appear black in the figures.

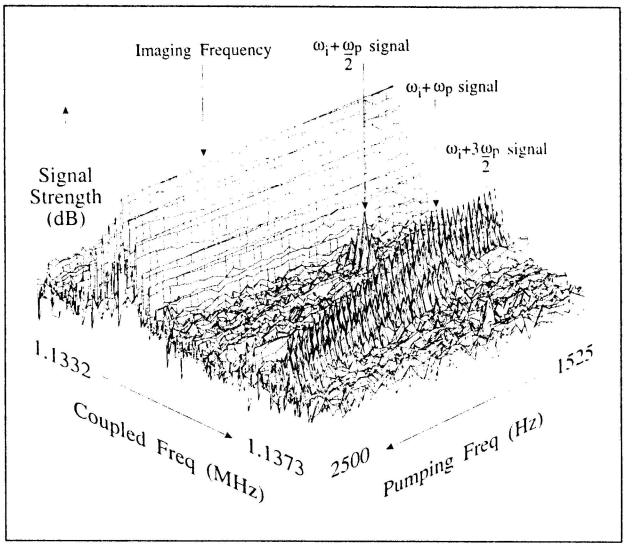

Figure 2. Mesh plot of the returned signal through a bubble's resonance using the full length combination frequency method. The bubble was insonified at 190 Pa (0-pk) and the pumping frequency was stepped in 25 Hz intervals.

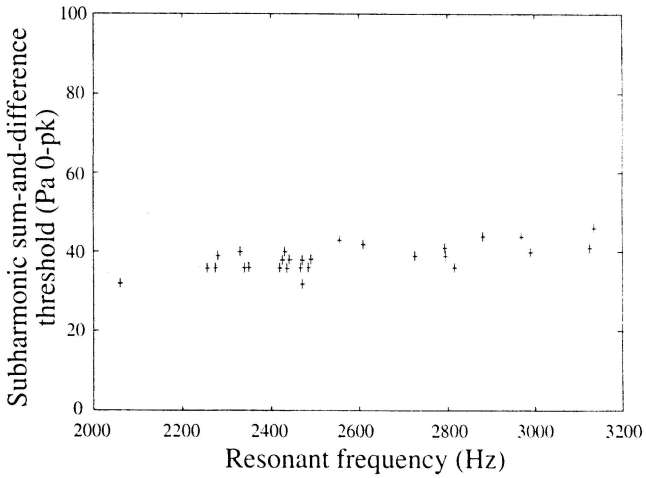

Figure 3. Plot showing the thresholds for sum-and-difference subharmonic excitation for various bubble sizes at 15 cm depth, measured in Pa (0-pk). Each point represents a single measurement, the more significant associated uncertainty being of the order ±3 Pa. The graph also shows the line of regression to the data

insonified at the slightly higher amplitude of 40 Pa. Clearly alternate high and low maxima in the modulation can be seen, and it is this which gives rise to signals at $\omega_i + \omega_p/2$.

A typical result from the experimental work is presented in Figure 2. Here a bubble was tethered to a horizontal wire at 15 cm depth in the focus of the transducers, and was simultaneously insonified with a 1.134 MHz imaging sound field and a pumping sound field which went between 1525 Hz and 2500 Hz in discrete 25 Hz steps. The amplitude of the pump signal was 190 Pa for each frequency, as the equipment/transducer/tank combination had been previously calibrated to allow inversion of its frequency response. The plot shows the measured response over a narrow frequency window (1.1332 to 1.1370 MHz), demonstrating the constant imaging frequency over all forty pump outputs, as well as several side lobes caused by an imperfection in the signal generator. However, these lobes are located within 400 Hz of the main beam, and so can clearly be distinguished from signals relating to the bubble's presence. To the right of this imaging signal is a broken ridge which is similarly present over all forty pumping signals – this is the 'sum' side of the coupled response corresponding to signals with components at $\omega_i + \omega_p$, and shows a slow rise to a maximum value at around $\omega_p/2\pi = 1800$ Hz. Between the two bands is a single peak which occurs at a pumping frequency of 1850 Hz. This is due to the subharmonic oscillation from the bubble, and is located at $\omega_i + \omega_p/2$. This clearly demonstrates the accuracy benefit of using the subharmonic coupled signal as an indicator of bubble resonance over the direct coupled signal.

Using heterodyning techniques to speed up the data collection and processing, the parametric characteristics of this subharmonic emission were investigated to locate the pumping signal amplitude at which the emission arose. This was performed by stepping through the bubble resonance in discrete 5 Hz steps at a constant amplitude level, calculating the height of the returned signal at the speculative location of the subharmonic signal component for each pump frequency, and then repeating the scan at a slightly higher signal amplitude. As the data collection and processing was completely automated, each amplitude scan took approximately 20 seconds, and the bubble could be completely characterised in around 8 minutes. This was performed on thirty individual tethered bubbles with resonance frequencies between 2000 Hz and 3200 Hz, and the amplitude locations of the subharmonic onset threshold are shown in Figure 3, along with the line of regression to the data.

This plot shows there is an apparently repeatable onset threshold of around 40 Pa with an associated error of the order of ±3 Pa for each point due to small uncertainties in the spatial positioning of the calibration transducer and the individual bubbles. The least squares fit straight line shows a rise in the threshold as the bubble resonance frequency increases, although this apparent gradient may not be statistically significant. The combination frequency subharmonic emission was verified using free rising bubbles, and it was found to exist and have a onset threshold of the same order of amplitude, although it was impossible to accurately quantify this threshold due to the transient nature of the events.

3. Theoretical Modelling And Simulation Results

3.1. A Bifurcation In The Volumetric Pulsations

As a bubble is driven at high amplitude, there is a potential for the volumetric pulsations to bifurcate as the system becomes more chaotic in behaviour [17]. The first bifurcation would manifest itself as two alternate maxima in the radius-time trace, and give rise to a signal content at half the driving

ACUSTICA · acta acustica
Vol. 83 (1997)

frequency. This possibility was examined using the Gilmore-Akulichev model for bubble dynamics. This is a nonlinear equation of motion which must be solved numerically, which for these tests used a fourth order Runge-Kutta solution with a step size control algorithm to maintain a user-specified round-off error. The basic form of the equation is:

$$\frac{\mathrm{d}U}{\mathrm{d}t} = \frac{1}{R\left(1-\frac{U}{c_L}\right)}\left[\left(1+\frac{U}{c_L}\right)H - \frac{3U^2}{2}\left(1-\frac{U}{3c_L}\right)\right] + \frac{1}{c_L}\frac{\mathrm{d}H}{\mathrm{d}t}, \tag{2}$$

where U is the velocity of the bubble wall, R is the instantaneous bubble radius, c_L is the local speed of sound in the fluid at the bubble wall and H is the enthalpy of the surrounding fluid. The model was initially developed by Gilmore [18], following the Kirkwood-Bethe hypothesis [19] which assumed that the speed of sound in the liquid varied as a function of the bubble motion. The equation was extended by Akulichev [20] to obtain the pressure field around the bubble, and by Cramer [21], Church [22] and Choi et al. [23] to facilitate the collection of numerical solutions. The model includes for the three damping mechanisms: acoustic, viscous and thermal, and can be used to study high amplitude bubble behaviour, such as lithotripter shock wave pulses [24] and rectified diffusion [22]. A full description of the equations and implementation of the simulation process can be found elsewhere [25].

The output from the simulations are radius-time plots, radiated pressure-time plots, pressure and temperature-time plots and moles of gas within the bubble-time plots to allow for the inclusion of gas diffusion across the bubble wall. For the investigation of the volumetric pulsations, only the radius-time curves are required, greatly speeding up the processing time. The resonant frequency of a 1 mm radius bubble at 15 cm depth was calculated using equation (1) as 3308 Hz, and this was used in the simulations. The tests were performed in insonification amplitude steps of 10,000 Pa, from 10,000 Pa to 200,000 Pa. As the program assumes the bubble to be at rest at the start of each simulation, there is a transient decay time at the beginning of each run before the steady state results start, which necessarily slows the computation. The steady state radius-time curves for the tests corresponding to insonification amplitudes of 160,000 Pa, 170,000 Pa and 200,000 Pa are given in Figures 4(a) to (c).

From these results it is clear that a definite bifurcation in the radius-time curves does exist, between 160,000 and 170,000 Pa insonification amplitude level. It is also apparent that by 200,000 Pa a second bifurcation has occurred, as the steady state solution shows four possible radius amplitude levels. If the maximum value which the bubble radii reach for each steady state section are noted for each increased amplitude level, a bifurcation diagram can be plotted for the volumetric pulsation mechanism, and this is shown in Figure 5. Thus the Gilmore-Akulichev model for bubble pulsations does demonstrate a bifurcation for a bubble driven at its resonant frequency, which for a 1 mm radius bubble occurs at roughly 170,000 Pa insonification level. Therefore unless the model is exceptionally insensitive this is unlikely to be the generation mechanism for the observed signals at $\omega_i \pm \omega_p/2$.

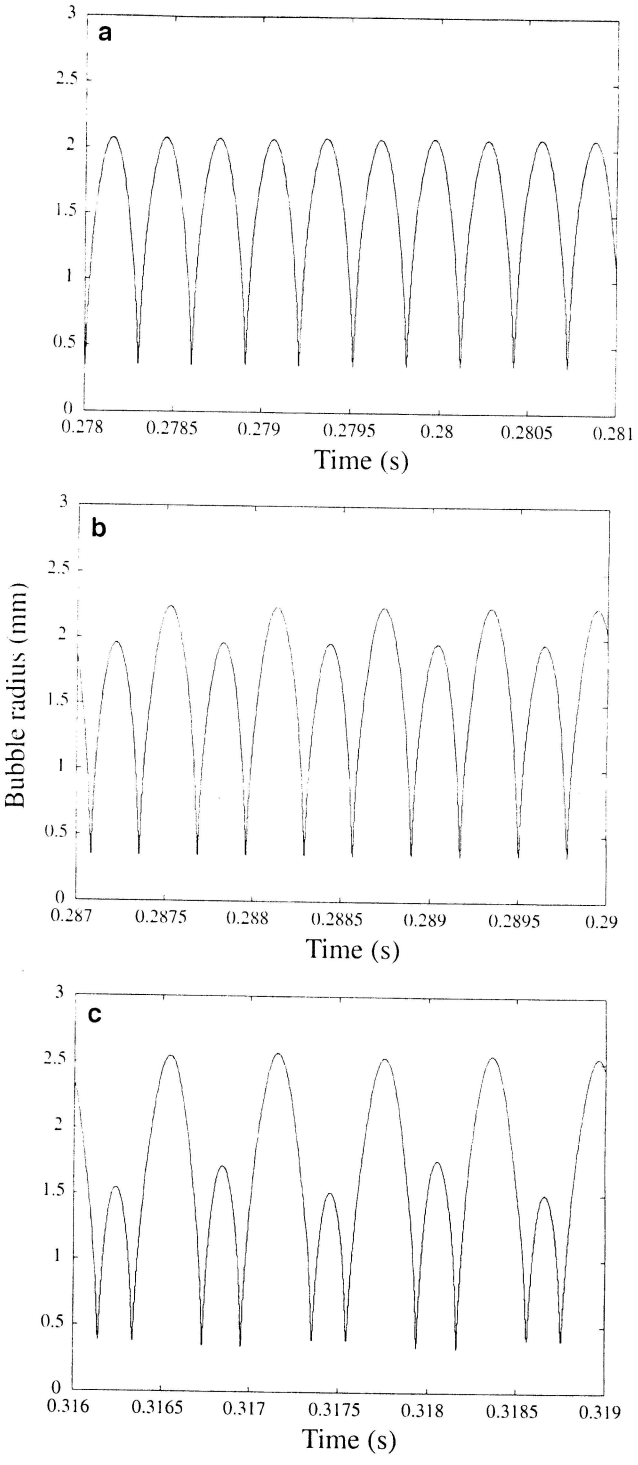

Figure 4. Gilmore Akulichev model of a 1 mm radius bubble driven at its resonance frequency of 3308 Hz. (a) Detail of the steady state radius time curve when the bubble was driven at 160,000 Pa (0-pk). (b) Detail of the steady state radius time curve when the bubble was driven at 170,000 Pa (0-pk). (c) Detail of the steady state radius time curve when the bubble was driven at 200,000 Pa (0-pk).

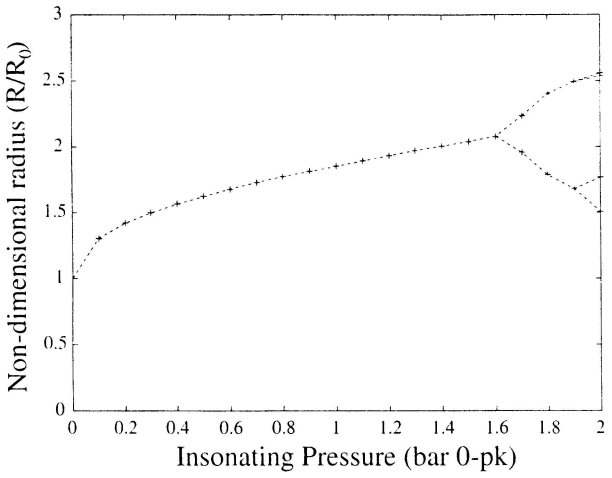

Figure 5. Bifurcation plot of the volumetric pulsation response for a 1 mm bubble driven at its resonance of 3308 Hz.

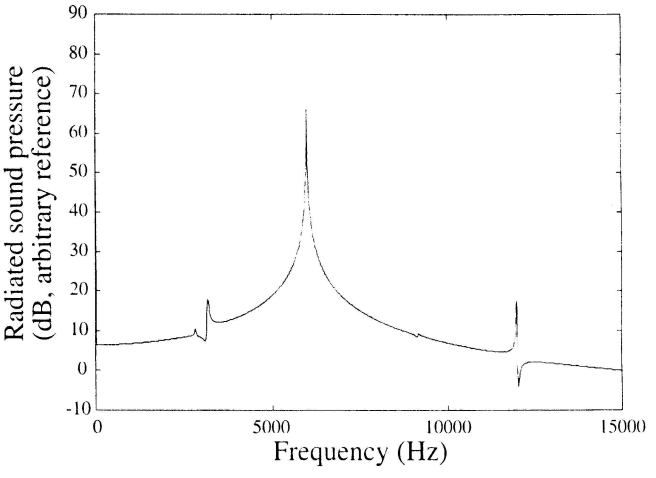

Figure 6. Frequency response of the radiated sound field calculated using the Gilmore Akulichev model for a 1 mm radius bubble driven by a 20,000 Pa (0-pk) sound field at twice its resonance frequency of 6616 Hz, to demonstrate the subharmonic onset using large bubble theory.

3.2. Large Bubble Theory

The second theory for subharmonic generation suggests that such emissions might be the result of the acoustic field acting on bubbles with an equilibrium radius twice the size of the radius resonant with the sound field, i.e. that the bubbles are being driven at twice their acoustic resonance frequency. This theory was first introduced by Eller and Flynn [11], who formulated a periodic solution to the Rayleigh-Plesset equation, and then tested the stability of the solutions by adding a small perturbation to the solution. This small perturbation is such that the resultant radial equation of motion will still satisfy the original Rayleigh-Plesset equation, but may not be periodic. Their theory presents a threshold for the subharmonic onset which is given by:

$$P_{T,A} = \frac{6 p_0 \Delta_{\log}}{\pi} \tag{3}$$

where $P_{T,A}$ is the acoustic pressure threshold for the signal, and $\Delta_{\log}$ is the logarithmic decrement representing the damping of the pulsation. Using Eller's equations [26] for the three damping terms of a pulsating bubble it can be calculated that a 1 mm radius air bubble in 15 cm depth of water at atmospheric pressure has a total non-dimensional damping coefficient of 0.13 when driven at twice its resonance frequency, and this gives a value for $\Delta_{\log}$ of 0.41. Substitution of this into equation (3) gives a subharmonic onset threshold value of approximately 80,000 Pa.

This work was continued by Prosperetti [12] who used similar theoretical techniques to predict the shape of the subharmonic onset curve in an attempt to better measure the damping characteristics of a pulsating bubble. He explains the origin of the subharmonic signal as a nonlinear coupling between different pulsation modes, with energy being transferred from the mode directly excited by the driving signal to the subharmonic mode. Prosperetti presents a plot (his Figure 3) which shows the onset amplitude of the subharmonic emission from a 1 mm bubble as a function of non-dimensional driving frequency, and which demonstrates a minimum when the bubble is driven at twice its resonant frequency, and with a threshold of approximately 40,000 Pa.

There appears to be a factor of two difference between the two onset thresholds. However, as both of the theoretical calculations presented above start from a linearised solution to the Rayleigh-Plesset equation, which is not an accurate model for such high amplitude bubble pulsations, a better estimate is possible. The Rayleigh-Plesset model assumes the bubble to be surrounded by an incompressible medium, and thus does not allow for acoustic radiation from the bubble into the fluid. This is an important damping mechanism of the volumetric pulsations [5]. Using the Gilmore-Akulichev model described earlier, which allows a variable speed of sound at the bubble wall, to numerically investigate the phenomenon, a potentially more accurate idea of the threshold location can be calculated. The same bubble parameters as those investigated in the earlier volumetric tests were used, except that the bubble was driven at 6616 Hz, twice the resonance frequency of a 1 mm radius bubble. The tests show the threshold to be at approximately 20,000 Pa, and data showing this signal is presented in Figure 6. The plot shows the Fourier Transform of the radiated sound field, and a clear signal approximately 50 dB lower than the backscattered response to the driving sound field is visible at 3 kHz. The plot shows the radiated sound pressure measured in decibels with an unspecified reference value, as only the relative heights of the peaks are important. However, while this is still lower than the earlier estimates and the volumetric pulsation threshold, it is clear that the threshold is still three orders of magnitude higher than the experimentally measured onset of the $\omega_i \pm \omega_p/2$ signal.

3.3. Onset Of Surface Waves

The earliest reported observation of a one-half subharmonic oscillation was made by Faraday [27]. He was investigat-

ACUSTICA · acta acustica
Vol. 83 (1997)

ing the motion of water over vibrating plates, in an effort to characterise the 'beautifully crispated appearance' of the liquid layer. To be able to fully observe the motion of the fluid layer, he built a board eighteen feet long, upon which a liquid layer 3/4 inches deep could be excited vertically. He observed the sloshing motion of 'heaps' of the liquid, such that 'each heap (identified by its locality) recurs or is reformed in two complete vibrations of the sustaining surface'. This result was confirmed by Rayleigh [28]. Neppiras [13] listed surface oscillations as a possible source of the subharmonic signal as they 'are excited parametrically, generally at half the excitation frequency.' But he argued that 'as the oscillations involve little or no volume change, it seems certain that they could not couple strongly enough into low-viscosity liquids to account for the strong signals observed'.

Calculating the driving amplitude onset threshold for these surface waves involves solving a Mathieu differential equation, and this has been evaluated numerically for a plane surface [29, 30]. This theory is extendible to bubbles provided that the wavelength of the surface disturbances is small compared with the circumference of the bubble [4]. Having established the surface wave amplitude threshold, it is reasonably simple to extend the theory to calculating the driving pressure amplitude. Eisenmenger [30] shows the origin of the Mathieu differential from the Navier-Stokes equation, demonstrates that the solution with the lowest pressure amplitude threshold predicts waves set up at half the driving frequency, and gives a threshold value of the plane surface displacement h_e which will give rise to these surface waves of:

$$h_e = \sqrt[3]{\frac{16\mu^3}{\sigma\rho^2\omega_A}}, \tag{4}$$

where ω_A is the acoustic driving frequency, and all the remaining symbols have their usual meanings. At 3 kHz, which is the rough frequency at which the experimental tests were performed, Eisenmenger also allows us to calculate the ratio of the surface wavelength to the bubble circumference, which can be evaluated as 0.09. Thus the surface displacements are more than 10 times smaller than the circumference, and so the plane surface assumption is approximately valid. Eller [26] presents a way of relating the acoustic pressure to the radial amplitude of a bubble, which when combined with equation (4), and equated at the bubble's resonance frequency gives a surface wave onset pressure threshold of:

$$P_{T,A} = \frac{6\mu\kappa p_0 d_{tot}}{R_0}\sqrt[3]{\frac{2}{\sigma\rho^2\omega_0}}, \tag{5}$$

where d_{tot} is the total non-dimensional damping coefficient. For a 1 mm bubble driven at resonance as described in the earlier simulations, this onset threshold can be calculated as 39 Pa. This is obviously very close to the experimentally measured values.

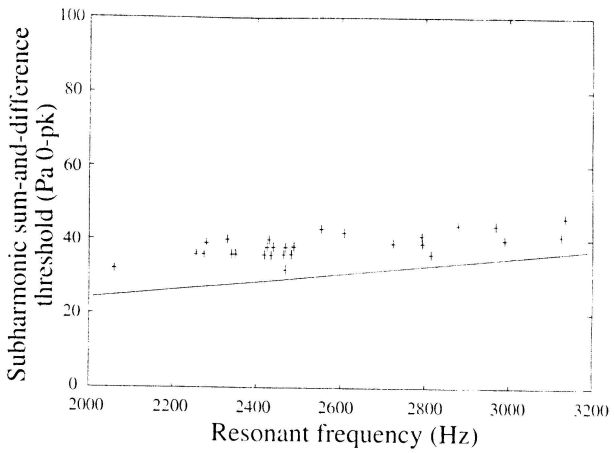

Figure 7. Plot showing the thresholds for subharmonic excitation for various bubble sizes at 15 cm depth, and their line of regression (dashed). The plot additionally shows the surface wave onset threshold (unbroken), calculated from plane-surface theory.

4. Discussion And Conclusions

It is clear that of the three potential mechanisms studied for the source of the subharmonic signal, the onset threshold for surface waves set up at half the driving frequency most closely matches the experimentally observed results. Figure 7 shows the theoretical threshold calculated over the range 2000 to 3200 Hz overlaid with the experimental results, and the plot shows good agreement between the theory and the experimental data, although there is a slight offset apparent, which may be because of the plane surface approximation in the threshold calculations.

In order to further check that these surface waves are present on a resonant bubble, close-up video photography was employed to record the pulsation characteristics of a driven tethered bubble. The experimental apparatus was placed into a clear PMMA (polymethylmethacrylate) water-filled tank inside a dark-room, and a bubble carefully tethered to a loop fashioned in a vertical wire. This bubble was then continuously insonified at its resonance frequency, and was simultaneously filmed using a Kodak Ektapro 1000 imager and processor fitted with a Monozoom 7E close-up lens as manufactured by Cambridge Instruments. The bubble was illuminated using a Griffin Model 65 Xenon stroboscope triggered by the video processor, with a flash time of 12 μs. The film was taken at 30 frames per second, and typical results are shown in Figures 8(a) and (b), for a bubble driven at resonance with a sound pressure level below the threshold necessary to generate a subharmonic emission, and for the same bubble insonified with a pressure amplitude above the subharmonic threshold. It is clear from Figure 8(b) that surface waves are evident around the bubble wall, which supports the theory that they are responsible for the $\omega_i \pm \omega_p/2$ signal. Also visible to the right in the two video frames is a ruler placed to facilitate optical cross-checks of the acoustic resonance estimates.

The greater width in the frequency domain of the $\omega_i \pm \omega_p$ signal compared with the $\omega_i \pm \omega_p/2$ signal suggests that the

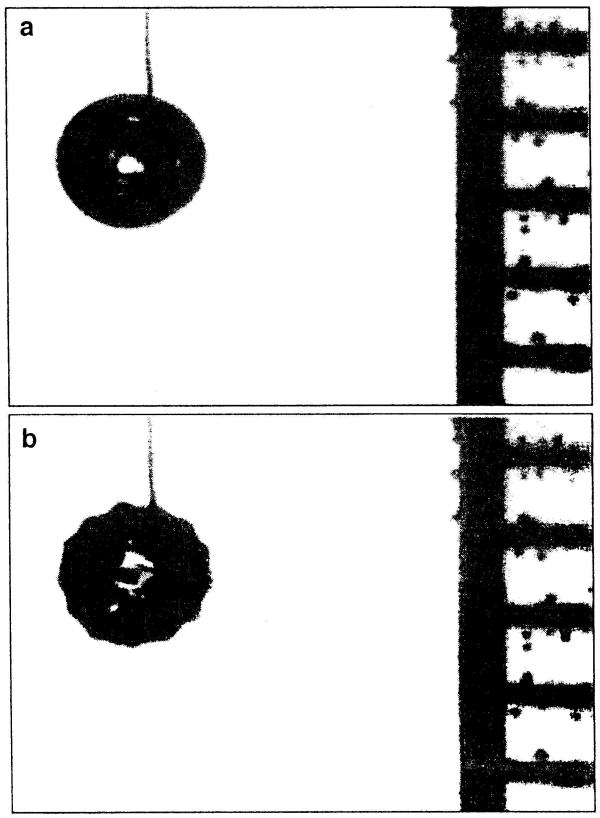

Figure 8. (a) Close-up video frame of an tethered bubble driven at resonance below the amplitude threshold necessary to generate a subharmonic emission. (b) Video frame of same bubble being driven above the subharmonic threshold, showing surface waves around the bubble wall. To the right in both pictures is a mm scale.

damping time constant associated with surface waves is less than that which relates to volumetric pulsations. Results published elsewhere [31], which show the variation in the height of the $\omega_i \pm \omega_p$ and $\omega_i \pm \omega_p/2$ signals as a function of the delay time included between the start of the insonification and the data acquisition, indicate that the maximum height of the $\omega_i \pm \omega_p/2$ signal is only reached after approximately 400 cycles of the driving sound field, while the $\omega_i \pm \omega_p$ signal maintains a constant height independent of this transient decay time. This implies that the damping mechanisms associated with the two signals are different, and that the subharmonic oscillation is very lightly damped as the start up transients persist over considerable time.

It was earlier discussed that the subharmonic emission should not propagate into the medium as no volumetric changes are brought about by the passage of surface waves around the bubble wall. However, the $\omega_i \pm \omega_p/2$ signal measured in the combination frequency tests at a distance from the bubble does not propagate in the same manner as the backscattered subharmonic signal. The ability of the subharmonic oscillation to couple efficiently with the imaging frequency to give strong sum-and-difference signals can be explained by looking at the mechanisms by which the two signals are nonlinearly mixed. Whereas monopole acoustic radiation by the subharmonic requires a volume change, its ability to couple to the imaging signal is a function of the geometric cross-sectional area of the bubble, and thus requires no volume change. If the returned signal from the two frequency insonified bubble is thought of as the output from a cyclo-stationary process, as detailed earlier, it is apparent that the strength of the backscatter is proportional to the cross-sectional area of the target presented to the beam. Therefore if the surface waves cause a modulation of this cross-sectional area at the subharmonic frequency, a signal containing a $\omega_i \pm \omega_p/2$ component will be returned. This can be illustrated using the results presented earlier in Figure 2, and in further results taken with the high frequency data collection and processing equipment which are published elsewhere [16]. The maximum heights of the $\omega_i \pm \omega_p/2$ signals are between 20 and 25 dB lower than the imaging frequency ridges, which correspond to a subharmonic frequency modulation in the cross-sectional bubble area of between 0.3 and 1 %. A comparison with the amplitude of the surface waves shown in the photograph given in Figure 8(b) shows this area modulation to be of the right order of magnitude.

Acknowledgement

The authors wish to thank the Natural Environment Research Council, reference GR3/09992, for funding, Dr Victor Humphrey from the School of Physics at the University of Bath for useful discussion and Drs Choi and Coleman at St. Thomas' Hospital, London for the Gilmore model C source code on which the Matlab programs were based. The high speed camera used for Figures 8(a) and (b) was obtained through an EPSRC grant reference GR/H79815, and the authors wish to thank Mr P. Goodyer from the Rutherford Appleton Laboratory and Dave Ramble for their assistance in taking the photographs.

References

[1] T. J. Lin, H. G. Donnelly: Gas bubble entrainment by plunging laminar liquid jets. AIChE J. **12** (1966) 563–571.
[2] D. R. Gross, D. L. Miller, A. R. Williams: A search for ultrasonic cavitation within the canine cardiovascular system. Ultrasound Med. and Biol. **11** (1985) 85–97.
[3] D. K. Woolf, S. A. Thorpe: Bubbles and the air-sea exchange of gases in near-saturation conditions. J. Marine Res. **49** (1991) 435–466.
[4] E. A. Neppiras: Acoustic cavitation. Phys. Rep. **61** (1980) 159–251.
[5] T. G. Leighton: The acoustic bubble. Academic Press, London, 1994.
[6] T. G. Leighton, D. G. Ramble, A. D. Phelps: Comparison of the abilities of multiple acoustic techniques for bubble detection. Proc. Sonar Signal Processing, Institute of Acoustics, Loughborough, UK, 1995. 149–160.
[7] R. Esche: Untersuchung der Schwingungskavitation in Flüssigkeiten. Acustica **2** (1952) 208–218.
[8] L. Bohn: Acoustic pressure variation and the spectrum in oscillatory cavitation. Acustica **7** (1957) 201–216.
[9] A. D. Phelps, T. G. Leighton: Acoustic bubble sizing using two frequency excitation techniques. Proc. 2nd Conf. on Underwater Acoustics, L. Bjørnø, editor. European Commission, 1994. 201–206.

ACUSTICA · acta acustica
Vol. 83 (1997)

[10] A. D. Phelps, T. G. Leighton: Automated bubble sizing using two frequency excitation techniques. Sea Surface Sound '94, M. J. Buckingham and J. R. Potter, editors. World Scientific, 1995. 332–341.

[11] A. I. Eller: Damping constants of pulsating bubbles. J. Acoust. Soc. Am. **47** (1970) 1469–1470.

[12] A. Prosperetti: Application of the subharmonic threshold to the measurement of the damping of oscillating gas bubbles. J. Acoust. Soc. Am. **71** (1977) 11–16.

[13] E. A. Neppiras: Subharmonic and other low-frequency emission from bubbles in sound-irradiated liquids. J. Acoust. Soc. Am. **46** (1969) 587–601.

[14] A. D. Phelps, T. G. Leighton: High resolution bubble sizing through detection of the subharmonic response with a two frequency excitation technique. J. Acoust. Soc. Am. **99** (1996) 1985–1992.

[15] V. L. Newhouse, P. M. Shankar: Bubble size measurements using the nonlinear mixing of two frequencies. J. Acoust. Soc. Am. **75** (1984) 1473–1477.

[16] A. D. Phelps, T. G. Leighton: Investigations into the use of two frequency excitation to accurately determine bubble sizes. Bubble Dynamics and Interface Phenomena. Proc. of an IUTAM symposium held in Birmingham, UK, 6-9 September 1993. J. Blake, J.M. Boulton-Stone and N.H. Thomas, editors. Kluwer Academic Press, 1993. 475–484.

[17] W. Lauterborn, J. Holzfuss: Acoustic chaos. Int. J. Bifurcation and Chaos **1** (1991) 13–26.

[18] F. R. Gilmore: The growth or collapse of a spherical bubble in a viscous compressible liquid. Report 26-4, California Institute of Technology, 1952.

[19] J. G. Kirkwood, H. A. Bethe: The pressure wave produced by an underwater explosion. OSRD Rep. No. 558, 1942.

[20] V. A. Akulichev. – In: High-intensity ultrasonic fields. L. D. Rozenburg (ed.). Plenum, New York, 1971, 239–259.

[21] E. Cramer: The dynamics and acoustic emission of bubbles driven by a sound field. – In: Cavitation and inhomogeneities in underwater acoustics. W. Lauterborn (ed.). Springer-Verlag, Berlin Heidelberg, 1980, 54–63.

[22] C. C. Church: Prediction of rectified diffusion during nonlinear bubble pulsations at biomedical frequencies. J. Acoust. Soc. Am. **83** (1988) 2210–2217.

[23] M. J. Choi, A. J. Coleman, J. E. Saunders: The influence of fluid properties and pulse amplitude on bubble dynamics in the field of a shock wave lithotripter. Phys. Med. Biol. **38** (1993) 1561–1573.

[24] C. C. Church: A theoretical study of cavitation generated by an extracorporeal shock wave lithotripter. J. Acoust. Soc. Am. **86** (1989) 215–227.

[25] A. D. Phelps: Characterisation of the subharmonic response of a resonant bubble using a two frequency technique. Dissertation. University of Southampton, UK, 1995.

[26] A. I. Eller, H. G. Flynn: Generation of subharmonics of order one-half by bubbles in a sound field. J. Acoust. Soc. Am. **46** (1969) 722–727.

[27] M. Faraday: On the forms and states assumed by fluids in contact with vibrating elastic surfaces. Phil. Trans. Roy. Soc. London **121** (1831) 319–340.

[28] Rayleigh: On the crispations of fluid resting upon a vibrating support. Phil. Mag., Ser. 5 **16** (1883) 50–58.

[29] V. I. Sorokin: The effect of fountain formation at the surface of a vertically oscillating liquid. Soviet Phys. - Acoust. **3** (1957) 281–291.

[30] W. Eisenmenger: Dynamic properties of the surface tension of water and aqueous solutions of surface active agents with standing capillary waves in the frequency range from 10 kc/s to 1.5 Mc/s. Acustica **9** (1959) 327–340.

[31] D. G. Ramble, T. G. Leighton: Comparison of the abilities of multiple acoustic techniques for bubble detection. ISVR Technical report No. 250, 1995.